

Formation of Co–Ni Alloy Superlattices Composed of Face-centered Cubic (FCC) and Hexagonal Close Packed (HCP) Atomic Layers Using a Rectangular Pulse Voltage

M. Saitou

University of the Ryukyus, Department of Mechanical Systems Engineering, 1 Senbaru Nishihara-cho Okinawa, 903-0213, Japan.

*E-mail: saitou@tec.u-ryukyu.ac.jp

Received: 3 December 2019 / *Accepted:* 16 January 2020 / *Published:* 10 March 2020

Co–Ni alloy superlattices composed of face-centered cubic (FCC) and hexagonal close packed (HCP) atomic layers were electrodeposited using rectangular pulse voltages of 0.85 and 1.1 MHz, respectively. The energy dispersive X-ray spectroscopy and X-ray diffraction (XRD) data demonstrated that the Co–Ni alloy superlattices electrodeposited at 0.85 and 1.1 MHz formed face-centered cubic (FCC) and hexagonal close packed (HCP) atomic layers containing 35.5 and 14.4 wt% Ni, respectively. In addition, the XRD analyses demonstrated that the Co–Ni alloy superlattices designed to exhibit the lattice constants of 0.5 and 1.0 nm showed one and two Bragg diffraction peaks, respectively, in the small-angle X-ray scattering region. The lattice constants calculated from the Bragg diffraction angles were approximately consistent with the designed lattice constants of 0.5 and 1.0 nm.

Keywords: Co–Ni alloy; Superlattice; FCC; HCP; Lattice constant

1. INTRODUCTION

Co–Ni thin films have attracted great attention because of their wide applications in spintronic devices [1], oxygen evolution catalysts [2], Li-ion battery electrodes [3], supercapacitors [4], superhydrophobic coatings [5], and nanowires [6–7]. In terms of magneto-crystalline anisotropy, hexagonal close-packed (HCP) Co–Ni alloy thin films are good candidates for high coercivity compared to face-centered cubic (FCC) Co–Ni alloy thin films [8].

Co–Ni alloy superlattice films formed by vapor growth show Kiessig oscillations in the small-angle X-ray scattering region, which can be attenuated by the interface roughness in these films [9]. In addition, these superlattice films composed of two Co-content atomic layers formed by electrodeposition have shown Bragg diffraction [10].

According to the Co–Ni alloy phase diagram [11], the phase transition from HCP to FCC occurs at 29 wt% Ni. Co–Ni alloy nanowires [12] and thin films [13] formed by electrodeposition adopt FCC and HCP crystal structures depending on the Ni content, as shown in the Co–Ni phase diagram. It was previously reported that the Ni content in Co–Ni thin films electrodeposited using a rectangular pulse current was dependent on the rectangular pulse current frequency, allowing the Co–Ni thin films to exhibit FCC or HCP crystal structures [14]. Herein, 0.85 and 1 MHz frequencies were used because Co–Ni thin films electrodeposited at 0.85 and 1 MHz adopt FCC and HCP crystal structures, respectively.

Hence, the aim of this study is to demonstrate that Co–Ni alloy superlattices composed of FCC and HCP atomic layers can be formed using rectangular pulse voltages with frequencies of 0.85 and 1.1 MHz frequencies.

2. EXPERIMENTAL SETUP

In the experimental setup, $15 \times 10 \text{ mm}^2$ copper and $50 \times 40 \text{ mm}^2$ carbon plates were used for the cathode and anode, respectively. One side of the copper plate was electrically insulated so as to be deposited only on the other side. The anode impedance was 27 times smaller than that of the cathode and was regarded as negligible. The copper plates had mirror-like appearances. An aqueous solution containing the following chemical compounds (mol L^{-1}) was prepared: $\text{NiSO}_4 \cdot 6\text{H}_2\text{O}$ 0.475, $\text{CoSO}_4 \cdot 7\text{H}_2\text{O}$ 0.475, and $\text{KNaC}_4\text{H}_4\text{O}_6 \cdot 4\text{H}_2\text{O}$ 0.65.

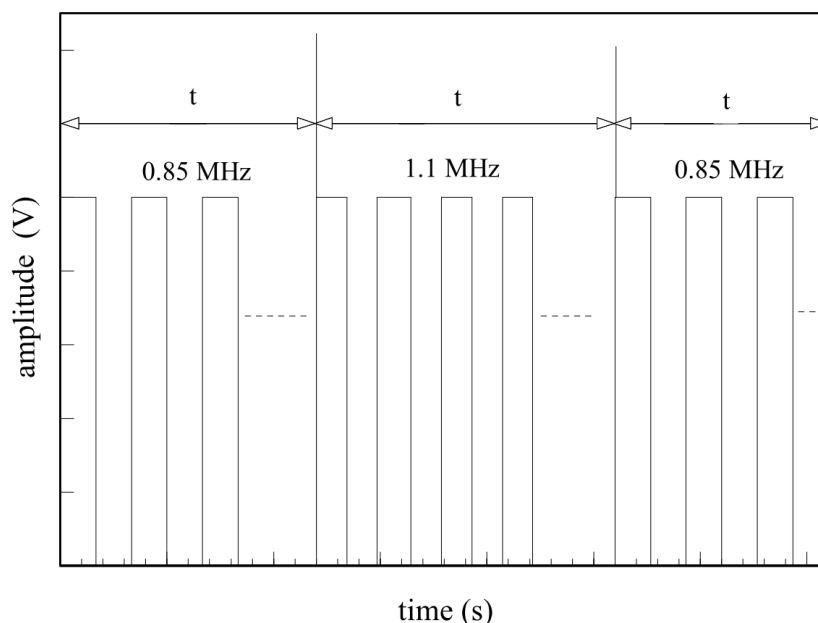


Figure 1. Schematic diagram of the rectangular pulse voltage used for electrodeposition of the Co–Ni alloy superlattice thin films. The symbol t denotes the time during which the rectangular pulse voltages with frequencies of 0.85 and 1.1 MHz were applied to the cell.

The cathode and anode were placed parallel to each other in a cell filled with the aqueous solution and maintained at 300 K during electrodeposition.

Rectangular pulse voltages with 0.85 and 1.1 MHz frequencies were applied to the cell using a function generator. A 22 Ω metal film resistor was connected in series with the cell to calculate the current flowing to the cell. The impedance of the metal film resistor was independent of the frequency at < 80 MHz.

Figure 1 shows a schematic diagram of 0.85 and 1.1 MHz rectangular pulse voltages flowing to the cell over a period, t . The unit lattice of the Co–Ni alloy superlattice was electrodeposited on the copper plate during the time $2t$.

After electrodeposition, the Co–Ni alloy superlattice films on the copper plates were rinsed with distilled water. The elemental contents of the Co–Ni alloy superlattices on the copper plate were determined using energy dispersive X-ray spectroscopy (EDX: Hitachi TM3030). The crystallographic textures of the Co–Ni alloy superlattices were determined using X-ray diffraction (XRD: Rigaku Ultima) with $\text{CuK}\alpha$ radiation.

3. RESULTS AND DISCUSSION

Oscillatory changes of the Ni content in the Co–Ni thin films deposited at 0.3–1.2 MHz have been reported using a rectangular pulse voltage [14].

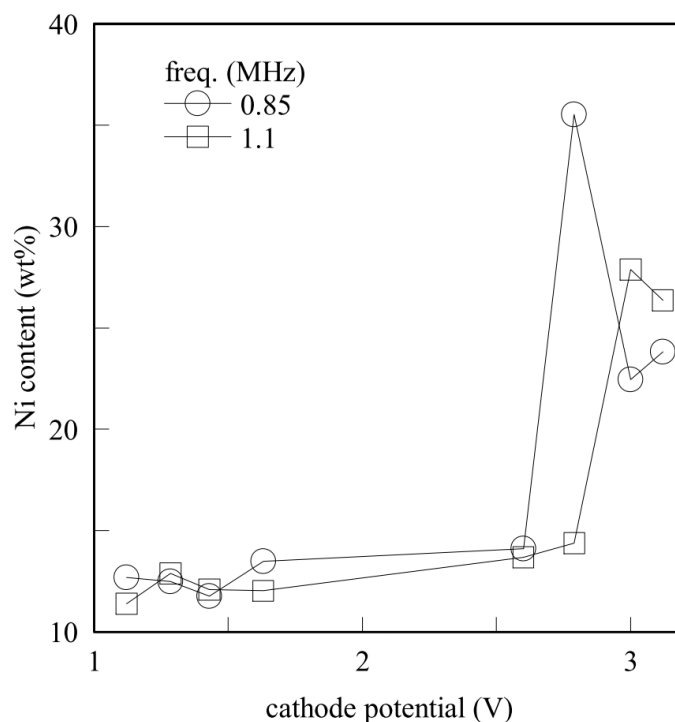


Figure 2. Plot of the Ni content vs. the cathode potential in Co–Ni thin films electrodeposited at 0.85 and 1.1 MHz.

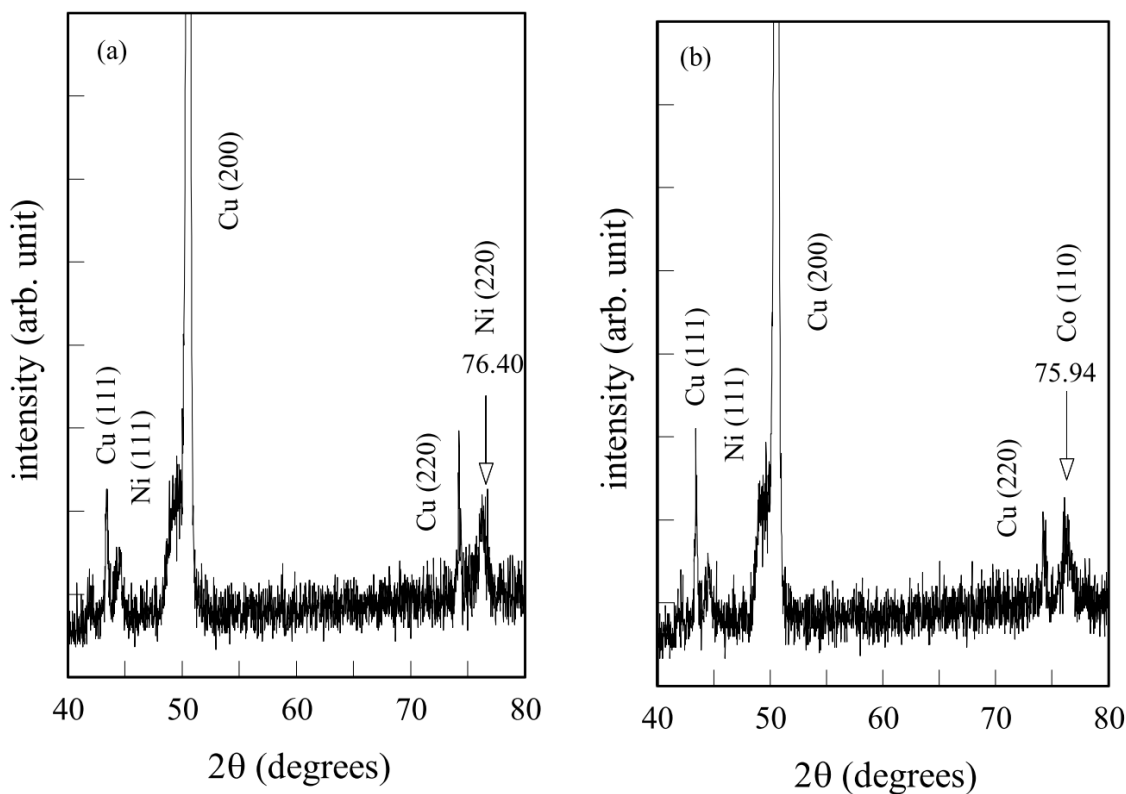


Figure 3. XRD charts of the Co–Mn thin films electrodeposited at (a) 0.85 and (b) 1.1 MHz.

However, the cathode potential has not been examined when the Ni content oscillation occurs. Figure 2 shows a plot of the Ni content of the Co–Ni thin films electrodeposited at 0.85 and 1.1 MHz as a function of the cathode potential. Herein, the cathode potential was determined using the following relation,

$$\text{cathode potential} = \text{amplitude} - \text{voltage drop between the } 22\Omega \text{ resistor. (1)}$$

The anode potential was ignored because the anode impedance was 27 times smaller than that of the cathode. The impedance between the anode and cathode was also ignored because of the high solution content.

In Fig. 2, a large difference in the Ni content occurred at a cathode potential of 2.79 V, where significant oscillatory changes in the Ni content with frequencies were observed [14]. All experiments in this study were performed at a cathode potential of 2.79 V. A current density of 29.5 mAcm^{-2} was determined by measuring the voltage drop between the 22Ω metal film resistor. The EDX analysis showed that the Ni content in the Co–Ni thin films electrodeposited at 0.85 and 1.1 MHz were 35.5 and 14.4 wt% Ni, respectively.

Figure 3 shows XRD charts of the Co–Ni thin films electrodeposited at 0.85 and 1.1 MHz, respectively. The Bragg diffraction peak from the (220) planes at 76.40° in Fig. 3 (a) is consistent with that in Ni [15]. Hence, the Co–Ni thin film electrodeposited at 0.85 MHz has an FCC Ni crystal structure. According to the EDX analysis, the Ni content in the corresponding Co–Ni thin film was 35.5 wt%, as

supported by the Ni–Co alloys phase diagram [11], which shows that Co–Ni alloys containing > 29.0 wt% Ni adopt FCC crystal structures. The distance between the (110) planes is 0.25 nm, which was used to determine the time, t . In a similar manner, the Bragg diffraction peak at 75.94° in Fig. 3 (b) is consistent with that of Co [16]. According to the EDX analysis, the Ni content in the Co–Ni thin film was 14.4 wt%, which is supported by the Ni–Co alloys phase diagram that indicates that Co–Ni alloys < 29.0 wt% Ni adopt HCP crystal structures. The distance between the (110) planes is 0.125 nm, which was used to determine the time period t .

Co–Ni thin films electrodeposited using 0.85 and 1.1 MHz rectangular pulse voltages (as shown in Fig. 1) at a cathode potential of 2.79 V are expected to exhibit FCC and HCP crystal structures, respectively. Time periods t , of 0.05 and 0.1 s were determined under the assumption of Faraday’s law [17] using 29.5 mAcm^{-2} current density and distances between the (110) planes in HCP and FCC crystal structures of 0.125 and 0.25 nm, respectively.

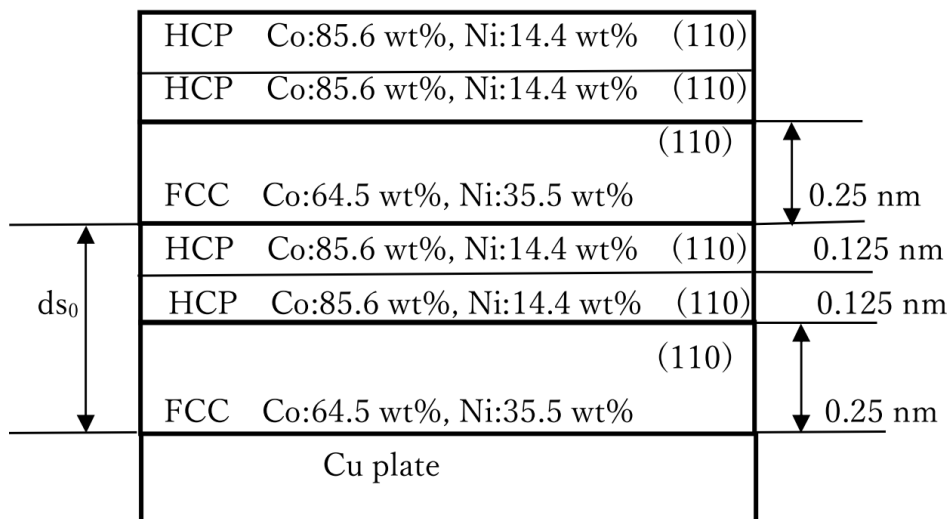


Figure 4. Schematic diagram of the unit lattice of the Co–Ni alloy superlattice structure that was expected for 2×0.05 s. Single and double Co–Ni alloy atomic layers containing 35.5 and 14.4 wt% Ni, respectively, were formed at 0.85 and 1.1 MHz over 0.05 s, alternately. The distances between the (110) planes of Ni (FCC) and Co (HCP) were determined to be 0.25 and 0.125 nm, respectively. The Co–Ni alloy superlattices showed a lattice constant of d_{s0} .

Figure 4 shows a schematic diagram of the unit lattice of the Co–Ni alloy superlattice formed at $t=2 \times 0.05$ s. A single FCC and double HCP atomic layers with (110) planes were formed at 0.85 and 1.1 MHz for 0.05 s, respectively, and the notation d_{s0} represents the lattice constant of the superlattice.

Figure 5 shows the XRD chart of the Co–Ni alloy superlattice thin film electrodeposited at $t=0.05$ s. The unit lattice of the Co–Ni alloy superlattice was composed of single FCC and double HCP atomic layers. The unit lattices of 6000 have a film thickness of $3.0 \mu\text{m}$. According to the standard diffraction intensity of Ni [15], the Bragg diffraction intensity from the (220) planes is 5 times weaker than that from the (111) planes. However, in Fig. 5 the Bragg diffraction intensity from the Ni (220) planes was approximately 4 times stronger than that from the Ni (111) planes. In a similar manner,

according to the standard diffraction intensity of Co [16], the diffraction intensity from the (110) planes is 1.3 times stronger than that from the (002) planes. However, in Fig. 5 the Bragg diffraction intensity from the Co (220) planes was approximately 4 times stronger than that from the Co (002) planes. Hence, the Ni (110) and Co (110) planes were dominant in the Co–Ni thin film as crystallographic planes parallel to the Cu plates.

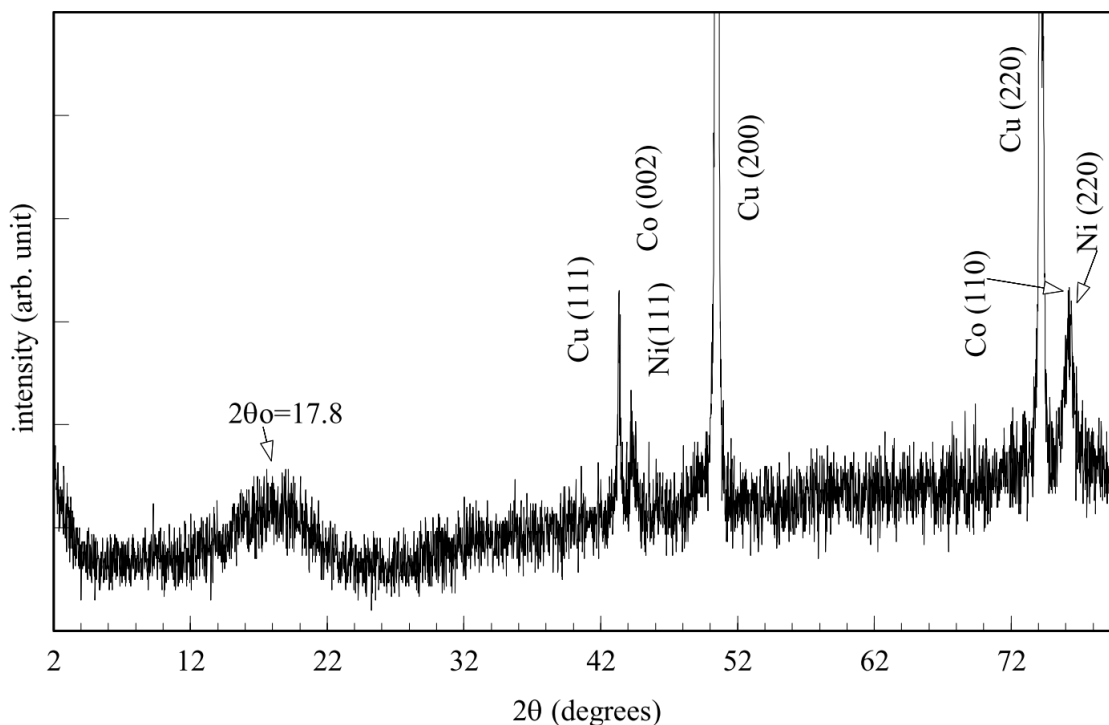


Figure 5. XRD chart of the Co–Ni alloy superlattice thin film electrodeposited using the time period, t of 0.05 s. The Co–Ni alloy superlattice thin film was composed of 6000 unit lattices.

The Cu plate appeared to be a mirror, but, was not smooth at the atomic level. During the initial stage of growth, the Co–Ni superlattice film filled gaps around the Cu rough surface, resulting in a static grain size will not increase. Hence, Co–Ni monolayers that could not grow layer by layer all over the surface showed distorted interfaces. The grain size and distorted Co–Ni superlattice caused the broad Bragg diffraction peak at 17.8° .

Using Bragg's formula $\lambda = 2d_{s0} \sin\theta$ where λ is the X-ray wave length, d_{s0} is the lattice constant of the super lattice, and θ is the incident angle of the X-ray, a d_{s0} value of 0.5 nm was obtained, consistent with the lattice constant reported in Fig. 5. Hence, it was confirmed that the Co–Ni superlattice film contained the Co–Ni superlattice, as expected from Fig. 4.

Figure 6 shows a schematic diagram of the unit lattice of the Co–Ni alloy superlattice structure formed at $t=2 \times 0.1$ s. Two FCC and four HCP atomic layers with (110) planes are formed at $t=0.1$. The notation d_{s1} represents the lattice constant of the superlattice. The notation d_{s2} is also the lattice constant of the superlattice, as it shows periodical structures containing one FCC and two HCP atomic layers.

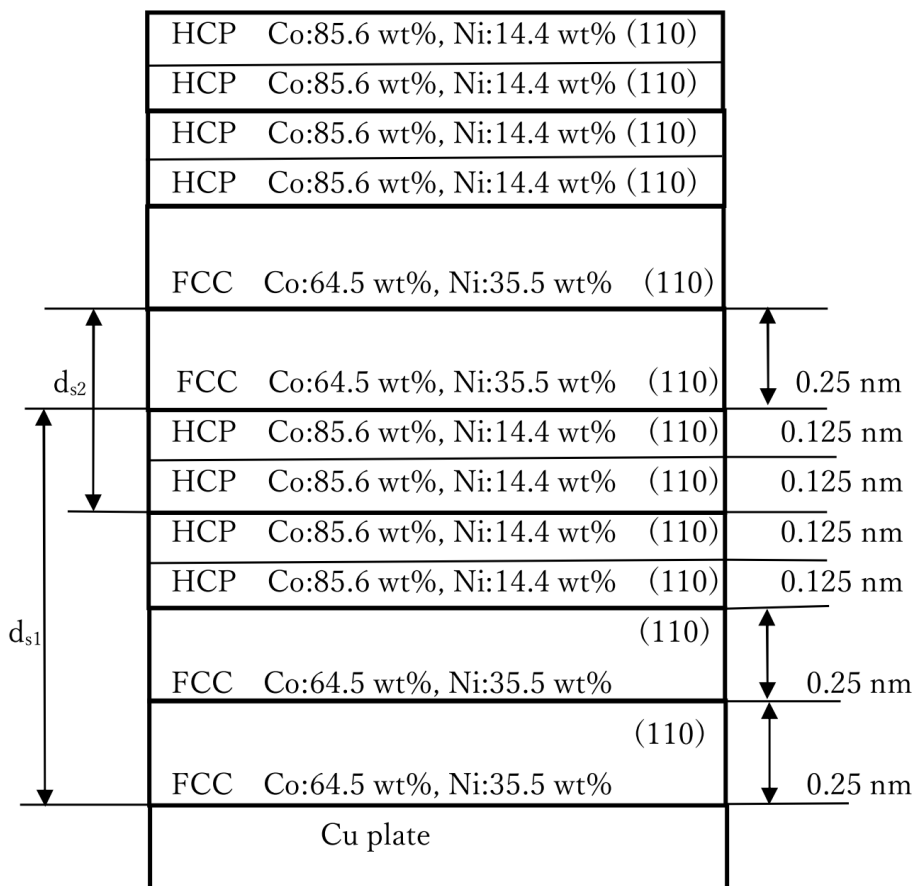


Figure 6. Schematic diagram of the unit lattice of the Co–Ni alloy superlattice structure expected at 2×0.1 s. Two and four Co–Ni alloy atomic layers containing 35.5 wt% and 14.4 wt% Ni, respectively, are grown at 0.85 and 1.1 MHz over a period of 0.1 s, alternately. The distances between the (110) planes of Ni (FCC) and Co (HCP) are 0.25 and 0.125 nm, respectively. The Co–Ni alloy superlattices are composed of two superlattices with lattice constants of d_{s1} and d_{s2} .

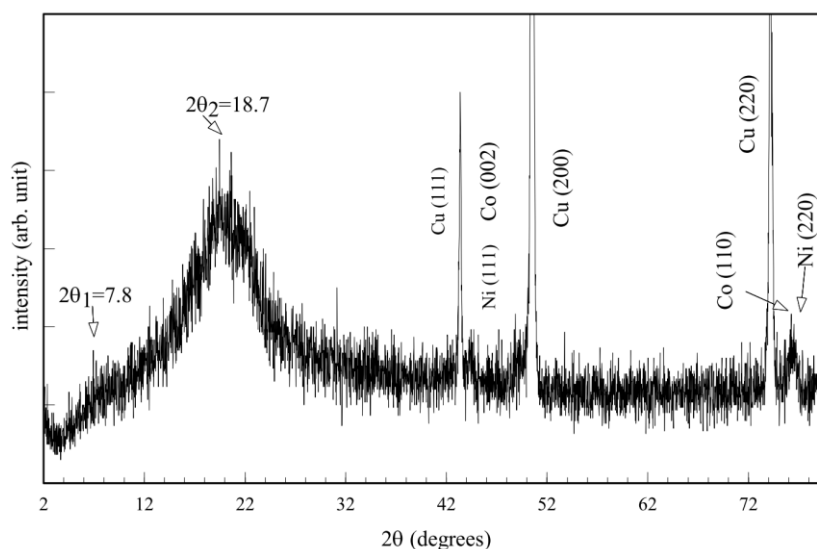


Figure 7. XRD chart of the Co–Ni alloy superlattice thin film electrodeposited using the time period, t of 0.1 s. The Co–Ni alloy superlattice thin film was composed of 3000 unit lattices.

Figure 7 shows the XRD chart of the Co–Ni alloy superlattice thin film electrodeposited at $t=0.1$ s. The number of the unit lattice with the lattice constant, d_{s1} was 3000 with a film thickness of $3.0 \mu\text{m}$. As the same reason stated in Fig. 6, the Ni (110) and Co (110) planes dominated as crystallographic planes parallel to the Cu plates.

Two broad Bragg diffraction peaks, i.e., weak and strong peaks emerged at 7.8 and 18.7° , respectively, owing to the interference intensity between the diffracted X-rays from the (110) planes. The peak from the superlattice with the long lattice constant, 1 nm was weak and that with the short lattice constant, 0.5 nm was strong. Using Bragg's formula $\lambda = 2d_{si}\sin\theta$ where $i=1$ or 2 , d_{s1} and d_{s2} were determined to be 0.47 and 1.1 nm , respectively, approximately consistent with the lattice constants shown in Fig. 6. Hence, the Co–Ni superlattice film was demonstrated to contain the Co–Ni superlattice as expected. The results are summarized in Table 1.

Table 1. Expected and calculated lattice constants

t (s)	expected lattice constant (nm)	calculated lattice constant (nm)
0,05	0.5	0.5
0.1	0.5 and 1.0	0.47 and 1.1

4. CONCLUSIONS

The Co–Ni superlattice films composed of HCP and FCC atomic layers were formed using 0.85 and 1.1 MH rectangular pulse voltages. The EDX and XRD analyses demonstrated that the lattice constants of the Co–Ni superlattice film formed over time periods of 0.05 and 0.1 s were approximately 0.5 and 1.0 nm , respectively, in agreement with the predicted values.

ACKNOWLEDGMENTS

The author thanks Mr K. Taira for the experimental setup.

References

1. S. Andrieu, T. Hauet, M. Gottwald, A. Rajanikanth, L. Calmels, A. M. Bataille, F. Montaigne, S. Mangin, E. Otero, P. Ohresser, P. Le Fèvre, F. Bertran, A. Resta, A. Vlad, A. Coati, and Y. Garreau, *Phys. Rev. Mater.*, 2 (2018) 064410.
2. X. Li, T. Wang, and C. Wang, *J. Alloy. Compd.*, 729 (2017) 19.
3. A. Dolati and S. S. Mahshid, *Appl. Surf. Sci.*, 276 (2013) 433.
4. J. Wang, Q. Zhong, Y. Xiong, D. Cheng, Y. Zeng, and Y. Bu, *Appl. Surf. Sci.*, 483 (2019) 1158.
5. Y. Xue, S. Wang, P. Bi, G. Zhao, and Y. Jin, *Coatings*, 9 (2019) 232.
6. R. Vidu, A. M. Predescu, E. Matei, A. Berbecaru, C. Pantilimon, C. Dragan, and C. Predescu, *Nanomater.*, 19 (2019) 1446.
7. Y. Chen, K. Maaz, S. Lyu, Y. Cheng, and J. Liu, *Physica E*, 322 (2017) 99.
8. M. Mohanta, S. K. Parida, A. Sahoo, Z. Hussain, M. Gupta, V. R. Reddy, and V. R. R. Medicherla,

- Physica B*, 572 (2019) 105.
9. D. Rafaja, J. Vacínová, and V. Valvoda, *Thin Solid Films*, 274 (2000) 10.
 10. M. Saitou, *Int. J. Electrochem. Sci.*, 14 (2019) 2383.
 11. A. F. Guillermet, *Z. Metallkd.*, 78 (1987) 639.
 12. A. Mukhtar¹, B. S. Khan, T. Mehmood, *Appl. Phys. A*, 122 (2016) 1022.
 13. C. Liu, F. Su, and J. Liang, *Surf. Coat. Tech.*, 292 (2016) 37.
 14. M. Saitou, *Int. J. Electrochem. Sci.*, 13 (2018) 305.
 15. *JCPDS-ICDD Card*, No. 04-0850
 16. *JCPDS-ICDD Card*, No.5-0727
 17. R. K. Pandey, S. N. Sahu, and S. Chandra, *Handbook of Semiconductor Electrodeposition*, Marcel Dekker, Inc., New York, 1996.

© 2020 The Authors. Published by ESG (www.electrochemsci.org). This article is an open access article distributed under the terms and conditions of the Creative Commons Attribution license (<http://creativecommons.org/licenses/by/4.0/>).